Letter

Coherence-enhanced quantum-dot heat engine

Jaegon Um,[1,*] Konstantin E. Dorfman,[2,3,4,†] and Hyunggyu Park[5,6,‡]
[1]*Department of Physics, Pohang University of Science and Technology, Pohang 37673, Korea*
[2]*State Key Laboratory of Precision Spectroscopy, East China Normal University, Shanghai 200062, China*
[3]*Collaborative Innovation Center of Extreme Optics, Shanxi University, Taiyuan, Shanxi 030006, People's Republic of China*
[4]*Himalayan Institute for Advanced Study, Unit of Gopinath Seva Foundation, MIG 38, Avas Vikas, Rishikesh, Uttarakhand 249201, India*
[5]*School of Physics, Korea Institute for Advanced Study, Seoul 02455, Korea*
[6]*Quantum Universe Center, Korea Institute for Advanced Study, Seoul 02455, Korea*

(Received 7 December 2021; accepted 2 August 2022; published 25 August 2022)

We show that quantum coherence can enhance the performance of a continuous quantum heat engine in the Lindblad description. We investigate the steady-state solutions of the particle-exchanging quantum heat engine, composed of degenerate double quantum dots coupled to two heat baths in parallel, where quantum coherence may be induced due to interference between relaxation channels. We find that the engine power can be enhanced by the coherence in the nonlinear response regime, when the symmetry of coupling configurations between dots and two baths is broken. In the symmetric case, the coherence cannot be maintained in the steady state, except for the maximum interference degenerate case, where initial-condition-dependent multiple steady states appear with a dark state.

DOI: 10.1103/PhysRevResearch.4.L032034

Introduction. Quantum thermodynamics is an emerging field in view of the significant progress of technology which allows one to scale down heat-energy converting devices to nanoscale where quantum effects become crucial [1]. Examples of such quantum heat engines (QHEs) include lasers, solar cells, and photosynthetic organisms, where, along with a few-level quantum structure [2–4], a phenomenon of quantum coherence plays an important role [5–10]. In particular, coherence in system-bath interactions that originates from the interference may enhance the power [11–13] and efficiency at maximum power [14] of the laser and solar cell and is responsible for highly efficient energy transfer in photosynthetic systems [15]. These effects have been confirmed in the experimental studies of polymer solar cells [16]. The noise-induced coherence is different from the internal coherence in the system Hamiltonian [17], which was recently demonstrated in the nitrogen-vacancy-based microscopic QHE in diamond [18], and manifests as an improved efficiency in spectroscopic pump-probe measurements [19].

So far, the majority of quantum coherence effects has been studied in continuously working bosonic devices [11,12,14,15,20]. Here, we focus on the fermionic QHE autonomously working without an external source, such as driving laser, made up of repulsively interacting double quantum dots with the degenerate energy levels, coupled to fermionic baths in parallel, depicted in Fig. 1. In contrast to previous studies [21–24], we introduce a parameter for the strength of interference between relaxation channels, which plays a crucial role. We derive the condition for maintaining quantum coherence in the steady state and investigate the engine performance, controlled by the tunneling coefficients between dots and baths and the interference strength.

We find that the power enhancement of the QHE can be achieved in the nonlinear response regime [25]. When coupling configurations assigned to each bath are symmetric, a quantum coherence initially induced by interference between relaxation channels would eventually disappear in the long-time (steady-state) limit. The exceptional case emerges for the degenerate energy level configuration at the maximum interference strength, when the dynamics is found to be localized, manifested as a mathematical singularity in the evolution operator evoking the so-called *dark* state [26], characterized by multiple steady states with finite quantum coherence depending on a given initial state. This singularity also emerges in more general settings with coherent dynamics originated from the energy-level degeneracy and parallel couplings, including a single bath case. Note that a spurious quantum coherence can be observed for a very long time (quasistationary state regime) near the maximum interference.

When the coupling configuration symmetry is broken in terms of either tunneling coefficients or interference strengths, a genuine new steady state emerges with nonvanishing quantum coherence, producing a *quantum current* between two baths through dots in addition to the conventional *classical* current. This quantum current yields an extra contribution to the engine power, which can be positive in a specific parameter regime.

Model. We first derive the quantum master equation (QME) [27] for the density operator $\hat{\rho}_S(t)$ of the fermionic QHE in the

*slung@postech.ac.kr
†dorfmank@lps.ecnu.edu.cn
‡hgpark@kias.re.kr

limit of weak coupling to hot (h) and cold (c) baths, where a temperature difference $T_\mathrm{h} - T_\mathrm{c} > 0$ and a potential bias $\mu_\mathrm{c} - \mu_\mathrm{h} > 0$ are applied. For simplicity, we assume a single energy level for each quantum dot with the degenerate energy levels $E_1 = E_2 = E$ and infinitely large repulsion between particles in dots. The system then can be described using three two-particle eigenstates: $|0\rangle$ denotes empty dots, and $|1\rangle$ and $|2\rangle$ stand for the occupation of dots 1 and 2, respectively, by a single particle. In addition, coherent hopping between dots is also forbidden and the only source of coherence is due to coupling to thermal baths.

The interaction between system and bath $a(=\mathrm{h},\mathrm{c})$ is given by $\hat{H}^a_\mathrm{SB} = \sum_{d,k} g^a_{dk}\hat{b}^{a\dagger}_k|0\rangle\langle d| + \mathrm{H.c.}$, where $\hat{b}^{a\dagger}_k$ is the operator creating a single particle with momentum k in bath a, and g^a_{dk} is the tunneling coefficient between dot $d(=1,2)$ and bath a. After tracing out bath degrees of freedom with the Born-Markov and the rotating wave approximations (RWA) [27,28], we obtain the QME which reads [29]

$$\partial_t\hat{\rho}_\mathrm{S} = -i[\hat{H}_\mathrm{S},\hat{\rho}_\mathrm{S}] + \sum_a\sum_{\alpha,\beta=1}^{4}\Gamma^a_{\alpha\beta}\left(\hat{L}_\alpha\hat{\rho}_\mathrm{S}\hat{L}^\dagger_\beta - \frac{1}{2}\{\hat{L}^\dagger_\beta\hat{L}_\alpha,\hat{\rho}_\mathrm{S}\}\right), \tag{1}$$

where the system Hamiltonian is $\hat{H}_\mathrm{S} = E(|1\rangle\langle 1| + |2\rangle\langle 2|)$ and the Lindblad operators are $\hat{L}_1 = |1\rangle\langle 0|$, $\hat{L}_2 = |2\rangle\langle 0|$, $\hat{L}_3 = \hat{L}^\dagger_1$, and $\hat{L}_4 = \hat{L}^\dagger_2$. Note that we neglected the Lamb shift term (see the Supplemental Material [30]). The dissipation matrix Γ^a is given by

$$\Gamma^a = \begin{pmatrix} w^a_{1+} & \phi^a\sqrt{w^a_{1+}w^a_{2+}} & 0 & 0 \\ \phi^{a*}\sqrt{w^a_{1+}w^a_{2+}} & w^a_{2+} & 0 & 0 \\ 0 & 0 & w^a_{1-} & \phi^{a*}\sqrt{w^a_{1-}w^a_{2-}} \\ 0 & 0 & \phi^a\sqrt{w^a_{1-}w^a_{2-}} & w^a_{2-} \end{pmatrix}, \tag{2}$$

where $w^a_{d\pm}$ represents the transfer rate of a particle between dot d and bath a; the subscript $+$ $(-)$ denotes the inflow (outflow) with respect to the dot. These rates are given by $w^a_{d+} = 2\pi|g^a_d|^2 N^a$ and $w^a_{d-} = 2\pi|g^a_d|^2\overline{N^a}$, where $g^a_d = g^a_d(E)$, $N^a = N^a(E)$ is the Fermi-Dirac distribution in bath a and $\overline{N^a} = 1 - N^a$ (see the derivation in Sec. S1 of the Supplemental Material (SM) [30]).

The off-diagonal terms in Eq. (2) represent interference between particle transfer associated with different dots. The interference effect is manifested as the nonzero off-diagonal terms of $\hat{\rho}_\mathrm{S}$, e.g., $\langle 1|\hat{\rho}_S|2\rangle \neq 0$. The coherence may not vanish even in the long-time limit due to the degeneracy; otherwise, it could be washed away under the RWA. In realistic experiments, however, the energy levels fluctuate in time due to fluctuations of gate voltages, which is not included in the system Hamiltonian. One expects that energy fluctuations around the degeneracy will result in partial coherence or dephasing [31], which can be phenomenologically added to our QHE model. Considering an observation of the exponentially decaying coherent current in a quantum-dot experiment [32], we introduce a phenomenological parameter ϕ^a representing a dephasing effect due to fluctuating energy levels in Eq. (2), assigned to each bath and which can be estimated experimentally (see Sec. S1 C of the SM [30]); $|\phi^a| = 1$ stands for permitting the full interference of relaxations with bath a, while $\phi^a = 0$ corresponds to no quantum effect of system-bath interactions. In earlier bosonic QHE models, ϕ^a is governed by the angle between dipole moments corresponding to two dots which ensures that $|\phi^a| \leqslant 1$ [11]. For convenience, ϕ^a is treated as a real number. Note that the second term in Eq. (1) is a standard form of the quantum dynamical semigroup [27], which guarantees the positive and trace-preserving dynamics since Γ^a in Eq. (2) is the positive-semidefinite matrix for $|\phi^a| \leqslant 1$.

To solve the QME, it is convenient to map the density operator to a vector: $\mathbf{P} = (\rho_{00},\rho_{11},\rho_{22},\rho_{12},\rho_{21},\rho_{01},\rho_{02},\rho_{10},\rho_{20})^\mathrm{T}$, where $\rho_{ij} = \langle i|\hat{\rho}_\mathrm{S}|j\rangle$. The last four components vanish in the long-time limit because there is no dynamics producing the coherence between the empty and occupied states so that only dephasing is allowed, as seen in Sec. S2 of the SM [30]. Thus, we write the corresponding Liouville equation as

$$\partial_t\mathbf{P} = \mathsf{L}\,\mathbf{P}, \tag{3}$$

where L is a 5×5 matrix with the reduced vector $\mathbf{P} = (\rho_{00},\rho_{11},\rho_{22},\rho_{12},\rho_{21})^\mathrm{T}$. Introducing $W_d = \sum_a w^a_{d+}$, $\overline{W}_d = \sum_a w^a_{d-}$, $\Phi = \sum_a \phi^a\sqrt{w^a_{1+}w^a_{2+}}$, and $\overline{\Phi} = \sum_a \phi^a\sqrt{w^a_{1-}w^a_{2-}}$, the L matrix then reads

$$\mathsf{L} = \begin{pmatrix} -W_1 - W_2 & \overline{W}_1 & \overline{W}_2 & \overline{\Phi} & \overline{\Phi} \\ W_1 & -\overline{W}_1 & 0 & -\overline{\Phi}/2 & -\overline{\Phi}/2 \\ W_2 & 0 & -\overline{W}_2 & -\overline{\Phi}/2 & -\overline{\Phi}/2 \\ \Phi & -\overline{\Phi}/2 & -\overline{\Phi}/2 & -\frac{\overline{W}_1+\overline{W}_2}{2} & 0 \\ \Phi & -\overline{\Phi}/2 & -\overline{\Phi}/2 & 0 & -\frac{\overline{W}_1+\overline{W}_2}{2} \end{pmatrix}. \tag{4}$$

Steady-state solutions. From the steady-state condition, $\mathsf{L}\mathbf{P}(\infty) = 0$, we find the relations as

$$\rho_{11}(\infty) = \frac{W_1\overline{W}_2 - \overline{\Phi}(W_2 + \overline{W}_2 - W_1)\rho_{12}(\infty)}{W_1\overline{W}_2 + \overline{W}_1 W_2 + \overline{W}_1\overline{W}_2},$$
$$\rho_{22}(\infty) = \frac{\overline{W}_1 W_2 - \overline{\Phi}(W_1 + \overline{W}_1 - W_2)\rho_{12}(\infty)}{W_1\overline{W}_2 + \overline{W}_1 W_2 + \overline{W}_1\overline{W}_2}, \tag{5}$$

with the population conservation $(\rho_{00} + \rho_{11} + \rho_{22} = 1)$ and

$$\rho_{12}(\infty) = \rho_{21}(\infty) = \frac{2\Phi - (2\Phi + \overline{\Phi})[\rho_{11}(\infty) + \rho_{22}(\infty)]}{\overline{W}_1 + \overline{W}_2}. \tag{6}$$

Note that the classical solution is recovered from Eq. (5), when the coherence term vanishes $[\rho_{12}(\infty) = 0]$. This classical *incoherent condition* is determined by Eq. (6) as

$$2\Phi\overline{W}_1\overline{W}_2 - \overline{\Phi}(W_1\overline{W}_2 + \overline{W}_1W_2) = 0, \tag{7}$$

which is obviously satisfied for the trivial case with $\Phi = \overline{\Phi} = 0$ (or, equivalently, $\phi^a = 0$). Note that the equilibrium case ($T_\mathrm{h} = T_\mathrm{c}$ and $\mu_\mathrm{h} = \mu_\mathrm{c}$) also satisfies this incoherent condition due to $W_d/\overline{W}_d = \Phi/\overline{\Phi}$ with $N^\mathrm{h} = N^\mathrm{c}$.

In general, Eqs. (5) and (6) leads to a 2×2 matrix equation for ρ_{11} and ρ_{22} as

$$\mathsf{L}_\mathrm{ss}\begin{pmatrix}\rho_{11}(\infty)\\ \rho_{22}(\infty)\end{pmatrix} = \begin{pmatrix}W_1 - (2\Phi\overline{\Phi})/(\overline{W}_1 + \overline{W}_2)\\ W_2 - (2\Phi\overline{\Phi})/(\overline{W}_1 + \overline{W}_2)\end{pmatrix}, \tag{8}$$

with

$$\mathsf{L}_\mathrm{ss} = \begin{pmatrix} W_1 + \overline{W}_1 - \frac{\overline{\Phi}(2\Phi+\overline{\Phi})}{\overline{W}_1+\overline{W}_2} & W_1 - \frac{\overline{\Phi}(2\Phi+\overline{\Phi})}{\overline{W}_1+\overline{W}_2} \\ W_2 - \frac{\overline{\Phi}(2\Phi+\overline{\Phi})}{\overline{W}_1+\overline{W}_2} & W_2 + \overline{W}_2 - \frac{\overline{\Phi}(2\Phi+\overline{\Phi})}{\overline{W}_1+\overline{W}_2}\end{pmatrix}. \tag{9}$$

Unless the determinant $|\mathsf{L}_\mathrm{ss}|$ vanishes, the steady-state solution is uniquely defined, which is given explicitly in Eq. (S29) of the SM [30].

We next consider a special *r-symmetric* configuration [22], where the couplings are symmetric for both baths, i.e., $g_2^\mathrm{h}/g_1^\mathrm{h} = g_2^\mathrm{c}/g_1^\mathrm{c} \equiv r$, leading to $w_{2\pm}^a/w_{1\pm}^a = r^2$. We take $r > 0$ for simplicity. Assuming an additional symmetry for the coherence parameter as $\phi^\mathrm{h} = \phi^\mathrm{c} \equiv \phi$, one can show $W_d/\overline{W}_d = \Phi/\overline{\Phi}$ even in nonequilibrium ($N^\mathrm{h} \neq N^\mathrm{c}$), satisfying the incoherence condition in Eq. (7). However, at the maximum interference ($|\phi| = 1$), the matrix L_ss becomes singular with $|\mathsf{L}_\mathrm{ss}| = 0$ and multiple steady-state solutions emerge, which will be discussed later. With the broken symmetry ($\phi^\mathrm{h} \neq \phi^\mathrm{c}$), the quantum coherence survives with a nonclassical solution [$\rho_{12}(\infty) \neq 0$]. In a more general case with $g_2^\mathrm{h}/g_1^\mathrm{h} \neq g_2^\mathrm{c}/g_1^\mathrm{c}$, the classical solution is still possible by adjusting ϕ^h and ϕ^c appropriately to satisfy the incoherent condition, but L_ss cannot be singular.

Steady-state currents. A particle current J_d^a representing the time increment of the particle density of dot d due to bath a can be obtained from Eq. (1) as

$$J_d^a = w_{d+}^a\,\rho_{00} - w_{d-}^a\,\rho_{dd} - \phi^a\sqrt{w_{1-}^a w_{2-}^a}\left(\frac{\rho_{12}+\rho_{21}}{2}\right). \tag{10}$$

In the steady state, J_d^a should be balanced by two reservoirs such that $J_d^\mathrm{h}(\infty) = -J_d^\mathrm{c}(\infty) \equiv J_d(\infty)$ and the total current is given by $J = \sum_d J_d(\infty)$. Transferring an electron from bath h to bath c, the electron gains the energy governed by the difference between the chemical potentials $\mu_\mathrm{c} - \mu_\mathrm{h}$, and thus the QHE power yields $P = (\mu_\mathrm{c} - \mu_\mathrm{h})J$. As the heat flux from bath h is given by $\dot{Q}^\mathrm{h} = (E - \mu_\mathrm{h})J$, the QHE efficiency does not vary with the particle current as $\eta = P/\dot{Q}^\mathrm{h} = (\mu_\mathrm{c} - \mu_\mathrm{h})/(E - \mu_\mathrm{h})$.

The particle current can be further separated into the classical and the quantum parts as

$$J_d(\infty) = J_d^\mathrm{cl} + \Psi_d\,\rho_{12}(\infty), \tag{11}$$

where $\phi^a = 0$ is set for the classical part in Eqs. (5) and (10) as

$$J_1^\mathrm{cl} = \frac{\Delta N}{|\mathsf{L}_0|}(2\pi)^2\big|g_1^\mathrm{h}\big|^2\big|g_1^\mathrm{c}\big|^2\overline{W}_2, \quad J_2^\mathrm{cl} = \frac{\Delta N}{|\mathsf{L}_0|}(2\pi)^2\big|g_2^\mathrm{h}\big|^2\big|g_2^\mathrm{c}\big|^2\overline{W}_1, \tag{12}$$

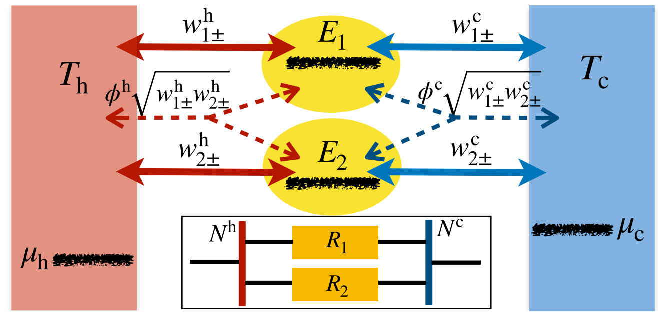

FIG. 1. A schematic illustration of the QHE, composed of two heat baths and a two-dot system. The dot energies, E_1 and E_2 (in this work, $E_1 = E_2$), are higher than the chemical potentials, μ_h and μ_c. $w_{d\pm}^a$ represents the transfer rate of a particle between dot d and bath a, and $\phi^a\sqrt{w_{1\pm}^a w_{2\pm}^a}$ denotes the interference amplitude. Inset: A circuit analogy of resistors in parallel.

with the external (bath) bias $\Delta N \equiv N^\mathrm{h} - N^\mathrm{c}$ and $|\mathsf{L}_0| = W_1\overline{W}_2 + \overline{W}_1W_2 + \overline{W}_1\overline{W}_2$ [$\mathsf{L}_0 = \mathsf{L}_\mathrm{ss}(\phi^a = 0)$], and $J_d^\mathrm{cl} > 0$ ensuring the positive power requires $\Delta N > 0$.

The second term represents the *quantum current* $J_d^\mathrm{q} \equiv \Psi_d\,\rho_{12}(\infty)$, induced by the coherence, and *quantum speed* Ψ_d and $\rho_{12}(\infty)$ are given in Sec. S3 of the SM [30]. Note that the quantum current for each dot can be both positive and negative, depending on the parameter values, as well as the total quantum current $J^\mathrm{q} = \sum_d J_d^\mathrm{q}$ (see Fig. S1 of the SM [30]).

As $\rho_{12}(\infty)$ is also proportional to bias ΔN, the QHE can be viewed as an analog of an electronic circuit with parallel resistors R_1 and R_2 under the external potential bias (see the inset of Fig. 1). The conductance σ_d of dot d is defined by the Ohm's law of $J_d(\infty) = \sigma_d\Delta N$, which is the reciprocal of resistance as $\sigma_d = R_d^{-1}$. The conductance is also divided into the classical and quantum parts as $\sigma_d = \sigma_d^\mathrm{cl} + \sigma_d^\mathrm{q}$ from Eq. (11). The classical part σ_d^cl is always positive, while the quantum part can be either positive or negative. In Fig. 2, we plot the relative quantum conductance $\sigma_d^\mathrm{q}/\sigma_d^\mathrm{cl}$ in the (ϕ^c, ϕ^h)

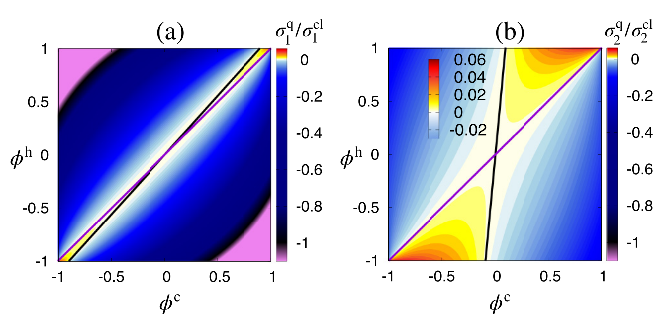

FIG. 2. Relative quantum conductances of (a) dot 1 and (b) dot 2, denoted as $\sigma_1^\mathrm{q}/\sigma_1^\mathrm{cl}$ and $\sigma_2^\mathrm{q}/\sigma_2^\mathrm{cl}$, respectively, in the ($\phi^\mathrm{c}$, ϕ^h) plane. Here, we used $N^\mathrm{h} = 0.2$ and $N^\mathrm{c} = 0.1$, and the r-symmetric configuration with $|g_1^a|^2 = 8\pi/(1 + r^2)$ and $|g_2^a|^2 = 8\pi r^2/(1 + r^2)$ at $r = 4$. Along the line of symmetry (purple), $\rho_{12}(\infty) = 0$, while $\Psi_d = 0$ defines the black line. The quantum conductances vanish along both lines. Note that a back flow [$J_d(\infty) < 0$] occurs near $\phi^\mathrm{h} = -\phi^\mathrm{c} = \pm 1$ in (a), where the negative quantum current overmatches the positive classical current.

plane in the r-symmetric configuration. Near but off the symmetric line of $\phi^{\rm h} = \phi^{\rm c}$, we find the total quantum conductance $\sigma^{\rm q} = \sum_d \sigma_d^{\rm q} > 0$, which means that the performance of the QHE can be enhanced beyond the classical limit in this parameter regime.

For small ΔN, we expand the relative quantum conductance as

$$\sigma_d^{\rm q}/\sigma_d^{\rm cl} = \mathcal{S}_d^0 + \mathcal{S}_d^1\,\Delta N + \cdots, \tag{13}$$

where $\mathcal{S}_1^0 \sim -(\phi^{\rm h} - \phi^{\rm c})^2$, $\mathcal{S}_2^0 = \mathcal{S}_1^0/r^2$, and $\mathcal{S}_d^1 \sim \phi^{\rm h}(\phi^{\rm h} - \phi^{\rm c})$ for the r-symmetric configuration (see Sec. S3 of the SM [30] for details). Interestingly, $\sigma_d^{\rm q}$ is always nonpositive in the linear response regime ($\mathcal{S}_d^0 \leqslant 0$), but may become positive due to $\mathcal{S}_d^1$ in the nonlinear regime as ΔN increases for $\phi^{\rm h}(\phi^{\rm h} - \phi^{\rm c}) > 0$. Note that $\mathcal{S}_d^1$ can dominate over $\mathcal{S}_d^0$ near the symmetric line ($\phi^{\rm h} = \phi^{\rm c}$). For $r > 1$, the negative quantum effect ($\mathcal{S}_d^0$) is relatively stronger for dot 1, which has a weaker coupling with baths, as also seen in Fig. 2, which might be applicable to a filtering circuit.

Although $\rho_{12}(\infty)$ becomes finite off the symmetric line ($\phi^{\rm h} \neq \phi^{\rm c}$), the quantum current may vanish again when $\Psi_d = 0$ in Eq. (11), which is denoted by black lines in Fig. 2. This can happen by balancing the quantum contributions from the stochastic part and the interference part, which are represented by the first two terms and the third term in the right-hand side of Eq. (10), respectively. The quantum enhancement occurs only between two lines of $\Psi_d = 0$ and $\rho_{12}(\infty) = 0$. For general cases outside of the r-symmetric configuration, these two lines are simply tilted (see Fig. S1 in the SM [30]), but the general features of the QHE are essentially unchanged.

Coupling-configuration symmetric case. We focus on the symmetric case with $\phi^{\rm h} = \phi^{\rm c} = \phi$ in the r-symmetric configuration, where $W_2 = r^2 W_1$, $\overline{W}_2 = r^2\overline{W}_1$, $\Phi = r\phi W_1$, and $\overline{\Phi} = r\phi\overline{W}_1$, yielding $W_d/\overline{W}_d = \Phi/\overline{\Phi}$. Then, the QME in Eq. (1) can be reduced to the single *effective* bath case, defined by a single coherence parameter ϕ and a rate W_1. A single bath typically enforces the system to reach a classical equilibrium state in the long-time limit. However, with degenerate energy levels, the off-diagonal (coherent) terms in the dissipation matrix Γ in Eq. (2) cannot be ignored even under the RWA. Thus, these coherent terms slow down the quantum dynamics significantly ($|\phi| < 1$), approaching the classical steady state via a long-lived quasistationary state with nonzero coherence.

We first calculate the eigenvectors $\mathbf{v}_i$ and the corresponding eigenvalues λ_i of the Liouville matrix L. Details are given in Sec. S4 of the SM [30]. We find the steady-state eigenvector $\mathbf{v}_1^{\rm T} = (\bar\alpha, \alpha, \alpha, 0, 0)$ with $\lambda_1 = 0$, where $\alpha = W_1/(2W_1 + \overline{W}_1)$ and $\bar\alpha = 1 - 2\alpha$, which corresponds to the classical fixed point. Other eigenvalues are negative except for $|\phi| = 1$, and thus the classical fixed point represents the unique steady state. At $|\phi| = 1$, however, another eigenvector $\mathbf{v}_4$ also has the zero eigenvalue, allowing multiple fixed points spanned by $\mathbf{v}_1$ and $\mathbf{v}_4$. Note that $|\mathsf{L}_{\rm ss}| = r^2(1 - \phi^2)(2W_1 + \overline{W}_1)\overline{W}_1$ from Eq. (9), which vanishes at these singular points of $|\phi| = 1$.

Defining a matrix $\mathsf{V} = (\mathbf{v}_1, \mathbf{v}_2, \mathbf{v}_3, \mathbf{v}_4, \mathbf{v}_5)$, the formal solution for $\mathbf{P}(t)$ reads

$$\mathbf{P}(t) = \mathsf{V}(1,\ \chi_2 e^{\lambda_2 t},\ \chi_3 e^{\lambda_3 t},\ \chi_4 e^{\lambda_4 t},\ \chi_5 e^{\lambda_5 t})^{\rm T}, \tag{14}$$

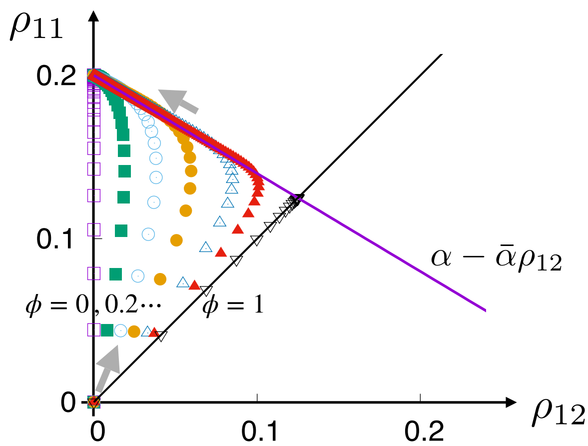

FIG. 3. Dynamic trajectories starting from $(\rho_{12}, \rho_{11}) = (0, 0)$ for various ϕ with $r = 1$, $W_1 = 0.25$, and $\overline{W}_1 = 0.75$, yielding $\alpha = 0.2$ and $\bar\alpha = 0.6$. Numerical data are denoted by various symbols for $\phi = 0, 0.2, 0.4, 0.6, 0.8, 0.9, 1$ (from left to right). The time interval between the same symbols is set to be 0.2 and the gray arrows denote the direction of the dynamics. The classical fixed point is at $(\rho_{12}, \rho_{11}) = (0, 0.2)$, while the coherent fixed point is at (0.125,0.125).

where χ_i depends on the initial condition $\mathbf{P}(0)$. At $|\phi| = 1$, $\lambda_1 = \lambda_4 = 0$, the steady state $\mathbf{P}(\infty)$ depends on $\mathbf{P}(0)$. In Fig. 3, we display typical dynamic trajectories in the (ρ_{12}, ρ_{11}) space with $r = 1$, starting from the empty initial condition of $\rho_{ij}(0) = 0$ except for $\rho_{00}(0) = 1$. As expected, all trajectories end up in the single (classical) fixed point in the long-time limit except for $|\phi| = 1$, where the new coherent fixed point appears with $\rho_{12}(\infty) \neq 0$. Note that the dynamics for $\phi \lesssim 1$ detours around the coherent fixed point for a significantly long time (quasistationary state), approaching the classical fixed point, which allows for experimental observation even in the presence of small decoherence.

The additional zero eigenvalue ($\lambda_4 = 0$) at the singular points ($|\phi| = 1$) implies another conservation law in addition to the probability conservation. Specifically, we find $r^2\dot\rho_{11} + \dot\rho_{22} - r\dot\rho_{12} - r\dot\rho_{21} = 0$ for $\phi = 1$ from Eq. (4), or $r^2\rho_{11}(t) + \rho_{22}(t) - r\rho_{12}(t) - r\rho_{21}(t) = I_0$ for all time t, where I_0 is a constant determined by the initial condition. We obtain the steady-state solutions using Eq. (5) and the conservation law, written as $\rho_{11}(\infty) = \alpha - [r\bar\alpha - \frac{1-r^2}{r}\alpha]\,\rho_{12}(\infty)$ and $\rho_{22}(\infty) = \alpha - [\frac{\bar\alpha}{r} + \frac{1-r^2}{r}\alpha]\,\rho_{12}(\infty)$, with

$$\rho_{12}(\infty) = \rho_{21}(\infty) = \frac{r}{1+r^2}\frac{1}{1-\alpha}\left(\alpha - \frac{I_0}{1+r^2}\right), \tag{15}$$

which depends on the initial state. In Fig. 3, we set $r = 1$ and $I_0 = 0$, so the coherent fixed point is determined by the intersection of two lines, $\rho_{11} = \rho_{12}$ and $\rho_{11} = \alpha - \bar\alpha\rho_{12}$. For $I_0 \neq 0$, the coherent fixed point is shifted along the curve of $\rho_{11} = \alpha - \bar\alpha\rho_{12}$. The case of $\phi = -1$ yields the same results except for changing the signs of ρ_{12} and ρ_{21} (see Eq. (S61) of the SM [30]). Note that the coherence can be finite and initial-state dependent even for $\Delta N = 0$ (equilibrium). This may raise a doubt that the quantum current $J_d^{\rm q}$

might not vanish in equilibrium, which is not the case since the quantum speed Ψ_d is proportional to bias ΔN (in fact, $\Psi_d = \phi(\frac{1+r^2}{r})J_d^{\rm cl}$ in Eq. (S62) of the SM [30]). The relative quantum conductance can be positive even in the linear response regime, i.e., $\mathcal{S}_d^0$ can be positive, depending on the initial state.

The phenomena of multiple fixed points responsible for a *dark* state emergence are observed in both fermionic [22] and bosonic [26,33] systems. Here, the system state can be recast in a rotated orthonormal basis as $|0\rangle$, $|+\rangle = (|1\rangle + r|2\rangle)/\mathcal{N}_r$, and $|-\rangle = (r|1\rangle - |2\rangle)/\mathcal{N}_r$ with $\mathcal{N}_r = \sqrt{1+r^2}$. Then, the system Hamiltonian is given as $\hat{H}_{\rm S} = E(|+\rangle\langle+| + |-\rangle\langle-|)$ and the interaction Hamiltonian becomes $\hat{H}_{\rm SB}^a = \mathcal{N}_r \sum_k g_{1k}^a \hat{b}_k^{a\dagger}|0\rangle\langle+| + {\rm H.c.}$ at the singular points. Note that the state $|-\rangle$ remains unchanged under the evolution operator, which corresponds to the dark state at $\phi = 1$, i.e., any initial population in the dark state remains intact or $\langle-|\hat{\rho}_{\rm S}|-\rangle = (r^2\rho_{11} + \rho_{22} - r\rho_{12} - r\rho_{21})/\mathcal{N}_r^2$ should be conserved. We can easily extend our result to the degenerate multiple dots with multiple occupancy allowed. As the dark state decouples with baths, it may be useful to protect quantum information from decoherence [34].

Note that the Lindblad description of degenerate quantum dots coupled to a single bath also yields multiple steady states with coherence at the maximum interference, in contrast with the common knowledge that a system coupled to a single bath should reach the incoherent thermal equilibrium, regardless of its initial state. Thus, the phenomenological parameter ϕ is natural to guarantee the thermal steady state for $|\phi| < 1$. Near the singular points, one may observe a long-living quasistationary state with the information of initial-state-dependent coherent solutions.

Conclusion. We investigated all possible steady-state solutions for the continuous quantum-dot QHE coupled to terminals in parallel for various tunneling coefficients and interference strengths. Here, the interference strength plays a similar role of the alignment of dipoles [35] in the bosonic system and acts as a source of decoherence. We found that unless the interference is completely negated, the steady states possess the coherence, which generates an extra quantum current, resulting in the enhanced QHE performance in a specific region of the parameter space, where the nonpositive linear quantum conductance is overcome by nonlinear contributions. We remark that a fine tuning of the parameter values is necessary for a significant enhancement such as the near symmetric coupling parameters. More enhanced QHE may require further investigation for the origin of nonlinear quantum conductance. Recently, the single-quantum-dot (fermion) heat engine was realized experimentally [36]. Since double-quantum-dot systems coupled to baths in parallel have been studied experimentally [37–39], the parallel-double-dot engine is also expected to be synthesized to confirm the enhancement of the QHE performance by thermal noises.

Acknowledgments. This research was supported by the NRF Grants No. 2020R1I1A1A01071924 (J.U.), No. 2017R1D1A1B06035497 (H.P.), and No. 2022R1I1A1A01063166 (J.U.), and by the KIAS individual Grant No. PG013604 (H.P.). K.E.D. is supported by the National Science Foundation of China (Grant No. 11934011), the Zijiang Endowed Young Scholar Fund, the East China Normal University, and the Overseas Expertise Introduction Project for Discipline Innovation (111 Project, Grant No. B12024).

[1] G. Benenti, G. Casati, K. Saito, and R. S. Whitney, Fundamental aspects of steady-state conversion of heat to work at the nanoscale, Phys. Rep. **694**, 1 (2017).

[2] M. O. Scully, M. S. Zubairy, G. S. Agarwal, and H. Walther, Extracting work from a single heat bath via vanishing quantum coherence, Science **299**, 862 (2003).

[3] R. Kosloff and A. Levy, Quantum heat engines and refrigerators: Continuous devices, Annu. Rev. Phys. Chem. **65**, 365 (2014).

[4] J. Jaramillo, M. Beau, and A. del Campo, Quantum supremacy of many-particle thermal machines, New J. Phys. **18**, 075019 (2016).

[5] H.-B. Chen, P.-Y. Chiu, and Y.-N. Chen, Vibration-induced coherence enhancement of the performance of a biological quantum heat engine, Phys. Rev. E **94**, 052101 (2016).

[6] R. S. Whitney, Quantum coherent three-terminal thermoelectrics: Maximum efficiency at given power output, Entropy **18**, 208 (2016).

[7] B. K. Agarwalla, J.-H. Jiang, and D. Segal, Quantum efficiency bound for continuous heat engines coupled to noncanonical reservoirs, Phys. Rev. B **96**, 104304 (2017).

[8] N. Brunner, M. Huber, N. Linden, S. Popescu, R. Silva, and P. Skrzypczyk, Entanglement enhances cooling in microscopic quantum refrigerators, Phys. Rev. E **89**, 032115 (2014).

[9] M. T. Mitchison, M. P. Woods, J. Prior, and M. Huber, Coherence-assisted single-shot cooling by quantum absorption refrigerators, New J. Phys. **17**, 115013 (2015).

[10] K. Hammam, Y. Hassouni, R. Fazio, and G. Manzano, Optimizing autonomous thermal machines powered by energetic coherence, New J. Phys. **23**, 043024 (2021).

[11] M. O. Scully, K. R. Chapin, K. E. Dorfman, M. B. Kim, and A. Svidzinsky, Quantum heat engine power can be increased by noise-induced coherence, Proc. Natl. Acad. Sci. USA **108**, 15097 (2011).

[12] Y. Yao, Spin-boson theory for charge photogeneration in organic molecules: Role of quantum coherence, Phys. Rev. B **91**, 045421 (2015).

[13] C. L. Latune, I. Sinayskiy, and F. Petruccione, Thermodynamics from indistinguishability: Mitigating and amplifying the effects of the bath, Phys. Rev. Research **1**, 033192 (2019).

[14] K. E. Dorfman, D. Xu, and J. Cao, Efficiency at maximum power of a laser quantum heat engine enhanced by noise-induced coherence, Phys. Rev. E **97**, 042120 (2018).

[15] K. E. Dorfman, D. V. Voronine, S. Mukamel, and M. O. Scully, Photosynthetic reaction center as a quantum heat engine, Proc. Natl. Acad. Sci. USA **110**, 2746 (2013).

[16] E. R. Bittner and C. Silva, Noise-induced quantum coherence drives photo-carrier generation dynamics at polymeric

semiconductor heterojunctions, Nat. Commun. **5**, 3119 (2014).

[17] R. Uzdin, A. Levy, and R. Kosloff, Equivalence of Quantum Heat Machines, and Quantum-Thermodynamic Signatures, Phys. Rev. X **5**, 031044 (2015).

[18] J. Klatzow, J. N. Becker, P. M. Ledingham, C. Weinzetl, K. T. Kaczmarek, D. J. Saunders, J. Nunn, I. A. Walmsley, R. Uzdin, and E. Poem, Experimental Demonstration of Quantum Effects in the Operation of Microscopic Heat Engines, Phys. Rev. Lett. **122**, 110601 (2019).

[19] Md. Qutubuddin and K. E. Dorfman, Incoherent control of optical signals: Quantum-heat-engine approach, Phys. Rev. Research **3**, 023029 (2021); Incoherent control of two-photon induced optical measurements in open quantum systems Quantum heat engine perspective, **4**, 023259 (2022).

[20] V. Holubec and T. Novotný, Effects of noise-induced coherence on the performance of quantum absorption refrigerators, J. Low Temp. Phys. **192**, 147 (2018).

[21] U. Harbola, M. Esposito, and S. Mukamel, Quantum master equation for electron transport through quantum dots and single molecules, Phys. Rev. B **74**, 235309 (2006).

[22] G. Schaller, G. Kießlich, and T. Brandes, Transport statistics of interacting double dot systems: Coherent and non-Markovian effects, Phys. Rev. B **80**, 245107 (2009).

[23] G. B. Cuetara, M. Esposito, and G. Schaller, Quantum thermodynamics with degenerate eigenstate coherences, Entropy **18**, 447 (2016).

[24] F. D. Ribetto, R. A. Bustos-Marún, and H. L. Calvo, Role of coherence in quantum-dot-based nanomachines within the Coulomb blockade regime, Phys. Rev. B **103**, 155435 (2021).

[25] A similar result was reported in a cyclic bosonic QHE; see K. Brandner, M. Bauer, and U. Seifert, Universal Coherence-Induced Power Losses of Quantum Heat Engines in Linear Response, Phys. Rev. Lett. **119**, 170602 (2017).

[26] V. V. Kozlov, Y. Rostovtsev, and M. O. Scully, Inducing quantum coherence via decays and incoherent pumping with application to population trapping, lasing without inversion, and quenching of spontaneous emission, Phys. Rev. A **74**, 063829 (2006).

[27] H.-P. Breuer and F. Petruccione, *The Theory of Open Quantum Systems* (Oxford University Press, New York, 2002).

[28] R. Alicki and R. Kosloff, Introduction to quantum thermodynamics: History and prospects, in *Thermodynamics in the Quantum Regime*, edited by F. Binder *et al.* (Springer, Cham, 2018), pp. 1–33.

[29] For the additivity of baths in the QME, see, also, X.-Q. Li, J. Y. Luo, Y.-G. Yang, P. Cui, and Y. J. Yan, Quantum master-equation approach to quantum transport through mesoscopic systems, Phys. Rev. B **71**, 205304 (2005); K. Ptaszyński, Coherence-enhanced constancy of a quantum thermoelectric generator, **98**, 085425 (2018); M. T. Mitchison and M. B. Plenio, Non-additive dissipation in open quantum networks out of equilibrium, New J. Phys. **20**, 033005 (2018).

[30] See Supplemental Material at http://link.aps.org/supplemental/10.1103/PhysRevResearch.4.L032034 for the derivation of the QME, eigenfunction analysis of the Liouville operator, calculations of steady-state currents, and analysis of the fully symmetric case.

[31] M. Q. Weng, Decoherence and relaxation in the interacting quantum dot system, Europhys. Lett. **85**, 17003 (2009).

[32] T. Hayashi, T. Fujisawa, H. D. Cheong, Y. H. Jeong, and Y. Hirayama, Coherent Manipulation of Electronic States in a Double Quantum Dot, Phys. Rev. Lett. **91**, 226804 (2003).

[33] J. Thingna, D. Manzano, and J. Cao, Dynamical signatures of molecular symmetries in nonequilibrium quantum transport, Sci. Rep. **6**, 28027 (2016).

[34] M. Zanner, T. Orell, C. M. F. Schneider, R. Albert, S. Oleschko, M. L. Juan, M. Silveri, and G. Kirchmair, Coherent control of a multi-qubit dark state in waveguide quantum electrodynamics, Nat. Phys. **18**, 538 (2022).

[35] A. A. Svidzinsky, K. E. Dorfman, and M. O. Scully, Enhancing photocell power by noise-induced coherence, Coher. Phenom. **1**, 7 (2012).

[36] M. Josefsson, A. Svilans, A. M. Burke, E. A. Hoffmann, S. Fahlvik, C. Thelander, M. Leijnse and H. Linke, A quantum-dot heat engine operating close to the thermodynamic efficiency limits, Nat. Nanotechnol. **13**, 920 (2018).

[37] A. W. Holleitner, C. R. Decker, H. Qin, K. Eberl, and R. H. Blick, Coherent Coupling of Two Quantum Dots Embedded in an Aharonov-Bohm Interferometer, Phys. Rev. Lett. **87**, 256802 (2001).

[38] A. W. Holleitner, R. H. Blick, A. K. Hüttel, K. Eberl, and J. P. Kotthaus, Probing and controlling the bonds of an artificial molecule, Science **297**, 70 (2002).

[39] J. C. Chen, A. M. Chang, and M. R. Melloch, Transition between Quantum States in a Parallel-Coupled Double Quantum Dot, Phys. Rev. Lett. **92**, 176801 (2004).